Assimilating atmospheric data into a terrestrial biosphere model: A case study of the seasonal cycle

T. Kaminski,[1,2] W. Knorr[1] P. J. Rayner,[3] and M. Heimann[1]

Received 16 July 2001; revised 6 March 2002; accepted 10 May 2002; published 24 October 2002.

[1] This paper demonstrates a new method of assimilating atmospheric concentration data into terrestrial biosphere models. Using a combination of adjoint and tangent linear models of both the underlying biosphere model and the atmospheric transport model, we directly infer optimal model parameters and their uncertainties. We also compute biospheric fluxes and their uncertainties arising from these parameters. We demonstrate the method using the Simple Diagnostic Biosphere Model (SDBM) and data on the seasonal cycle of CO_2 from 41 observing sites. In the model, the light-use efficiency for several biomes is well-constrained by concentration observations. Optimal values generally increase with latitude as required to match the seasonal cycle. Modeled Q_{10} values are poorly constrained unless local flux measurements are also used. Values also increase with latitude but are less than the commonly assumed value of 2. *INDEX TERMS:* 0315 Atmospheric Composition and Structure: Biosphere/atmosphere interactions; 1640 Global Change: Remote sensing; 1615 Global Change: Biogeochemical processes (4805); 3210 Mathematical Geophysics: Modeling; *KEYWORDS:* carbon cycle data assimilation, inverse modeling, adjoint, terrestrial biosphere, uncertainty analysis, atmospheric carbon dioxide

Citation: Kaminski, T., W. Knorr, P. J. Rayner, and M. Heimann, Assimilating atmospheric data into a terrestrial biosphere model: A case study of the seasonal cycle, *Global Biogeochem. Cycles*, *16*(4), 1066, doi:10.1029/2001GB001463, 2002.

1. Introduction

[2] The rising concentration of CO_2 [e.g., *Keeling et al.*, 1995] and its potential impact on climate are topics of substantial scientific and policy interest. Over the last 2 decades, much effort has been focused on understanding the processes which control the concentration of this gas in the atmosphere, as a possible prelude to managing the concentration. One tool commonly employed is atmospheric transport inversions [e.g., *Keeling et al.*, 1989; *Enting et al.*, 1995; *Rayner et al.*, 1999]. These studies seek to infer the net carbon exchange with the surface averaged over some time and space resolution, often continental or semihemispheric in spatial extent and at its finest at monthly timescales. Work by *Kaminski et al.* [1999b] is slightly different in that it infers fluxes at the resolution of the underlying transport model. As pointed out by [*Kaminski et al.*, 2001], this avoids a series of problems associated with trying to infer only large-scale fluxes.

[3] The relative sparsity of observations (maybe 100 monthly mean observations) and the poor sampling of large regions of the globe (e.g., tropical continents) means that these inversions are badly underdetermined. This underdeterminacy manifests itself as large uncertainties on individual regional fluxes. As we increase the horizontal resolution [e.g., *Kaminski et al.*, 1999b] the underdeterminacy becomes more apparent. This is true both because the number of unknown source components increases and also because atmospheric mixing dilutes signals from small regions faster than from large ones, making them harder to observe.

[4] It is still true that the $7.8^\circ \times 10^\circ$ resolution of *Kaminski et al.* [1999b] is too coarse for many policy applications, such as national carbon accounting. Hence if progress is to be made we need work on two fronts. The first is to open new streams of data, preferably guided so as to optimally improve our flux estimates. This has been approached incrementally by *Gloor et al.* [2000] with suggested expansions to the surface network, or more speculatively by *Rayner and O'Brien* [2001] with a suggested role for remotely-sensed concentration.

[5] The second obvious method is to try to increase the leverage of existing data. The simplest way to do this is to relate fluxes at one point to fluxes at another. As normally performed, synthesis inversion does this implicitly. These inversions use sources defined over large regions with patterns within the regions prescribed. Sources at every point in a region are adjusted by a single magnitude. Thus, even if only part of a region is observed by the measurement network, the sources at all points in the region are constrained. *Kaminski et al.* [2001] have demonstrated the problems with this approach if these prescribed patterns are incorrect.

[1]Max Planck Institut für Biogeochemie, Jena, Germany.
[2]Now at FastOpt, Hamburg, Germany.
[3]CSIRO Atmospheric Research, Aspendale, Victoria, Australia.

0886-6236/02/2001GB001463$12.00

[6] We can establish more subtle relationships between fluxes at different points. Such relationships are part of the task of models of surface processes. Such models consist of a series of variables describing the state of the system (such as the size of carbon pools) and a series of equations describing the evolution of that state. These evolution equations will usually contain parameters and the evolution of the state will depend on the values of these parameters as well as external forcing. Furthermore, any model will calculate quantities which may be observed, albeit indirectly. An example of such an observable is a surface flux from a terrestrial biosphere model. If we can use the observables to estimate the state at a particular time and the parameters of the system, then, subject to the veracity of the model equations themselves, we can describe the physical system.

[7] Such an approach was briefly sketched by *Rayner* [2001]. As mentioned there, it has a number of advantages. First, the description is likely to be more compact than a high-resolution description of many independent flux components. Hence, depending on the independent observability of the parameters and state variables, such a model is a powerful constraint in the inverse problem so that its drastic underdeterminacy may be ameliorated or even avoided.

[8] The second advantage is perhaps more important. In general, there has been a separation between the kinds of inferences made by atmospheric inversions and those from process models. This has been manifest as a so-called scale gap, where large-scale atmospheric inversions can only make usefully certain inferences at very large scales while process models can only be constrained by fairly small-scale observations (flux towers and the like). It has been difficult for the two communities to even disagree meaningfully. The approach outlined here may allow both kinds of estimate to infer the same kinds of quantity.

[9] The third advantage is to expand the list of observables treated by the inversion process. The atmospheric inversions carried out thus far have used two types of input, atmospheric constituent concentrations (including isotopes) and estimates of large-scale fluxes (e.g., from fossil-fuel combustion). These are optimally combined to produce improved estimates, usually for flux magnitudes. This ignores a large number of observables of the underlying processes, e.g., local flux measurements, satellite radiances, and biophysical variables. Combinations of satellite-derived vegetation indices and atmospheric concentrations have been previously used by *Knorr and Heimann* [2001] to check mutual consistency. The framework outlined here should allow the use of such multiple constraints in a traditional data assimilation mode.

[10] The final advantage of this approach is more ambiguous. In general, the estimation of model parameters avoids the distinction between prognostic and diagnostic investigations of the system. The flux estimates of previous inversion studies are purely diagnostic. They do not, of themselves, estimate quantities which will aid prediction. Process model studies, on the other hand, are largely prognostic, only the task of tuning these models involves a diagnosis of the current state. The approach of estimating model parameters and state variables should overcome this difference. Of course, if the underlying model is wrong, the inferred parameters, although producing an optimal match to current data, will yield meaningless predictions.

[11] The approach of estimating underlying parameters in process models from observations is not itself new. *Fung et al.* [1987] used atmospheric CO_2 concentrations to cross-check their model for inferring terrestrial productivity from satellite observations, an approach updated in the study of *Knorr and Heimann* [2001]. A new element of this study is that the satellite data themselves are used to constrain estimates of model parameters, a method also explored by *Knorr and Schulz* [2001]. *Knorr and Heimann* [1995] used atmospheric CO_2 concentrations to tune parameters in a terrestrial biosphere model while *Balkanski et al.* [1999] used the seasonal cycle of atmospheric O_2/N_2 ratios to tune parameters for an ocean biology model. Most recently, *Randerson et al.* [2002] used both CO_2 and $\delta^{13}C$ observations to constrain their values of isotopic discrimination at high latitudes. In general, these studies have adjusted the parameters by hand until they got a reasonable match with the concentration data. One exception is the study of *Vukićević et al.* [2001] which used a more formal variational technique (though without showing uncertainties) with a simple, globally averaged terrestrial model. The development path is similar to that of flux inversions. The landmark studies by *Keeling et al.* [1989] and *Tans et al.* [1990] used manual parameter adjustment. Later, the studies of *Enting et al.* [1995] introduced systematic methods for optimal parameter estimation. Most importantly, these systematic methods also allowed the calculation of the uncertainty of the flux magnitudes. We intend here to bring a similarly systematic approach to the estimation of model parameters, particularly a calculation, albeit incomplete, of their uncertainties.

[12] The outline of the rest of the paper is as follows: Section 2 describes the methodology in detail. Section 3 describes the underlying terrestrial model and atmospheric transport model, briefly, since they are both described elsewhere in the literature. Section 4 describes the results of the estimation of model parameters from a moderate-sized network of concentration observations. Section 5 tests some of the assumptions in our method, particularly the various linearizations for the uncertainty calculations. Finally, we sketch the application of this method to more challenging problems.

2. Assimilation Methodology

[13] The aim of our calculation is to infer some information (an estimate of the mean and uncertainty) about a set of parameters $\mathbf{p}$ from some atmospheric concentration observations $\mathbf{c}$. This involves the propagation of information in an inverse sense through a chain of models. This information flow is shown in a forward sense in Figure 1. Starting from the parameters themselves there is first a terrestrial biosphere model B which produces among other things a space-time distribution of modeled fluxes $\mathbf{f}_M$ on a $0.5 \times 0.5^\circ$ grid. Next is some kind of aggregation or interpolation process to take the fluxes and map them onto the $7.8 \times 10^\circ$ grid of the atmospheric transport model. We denote this as

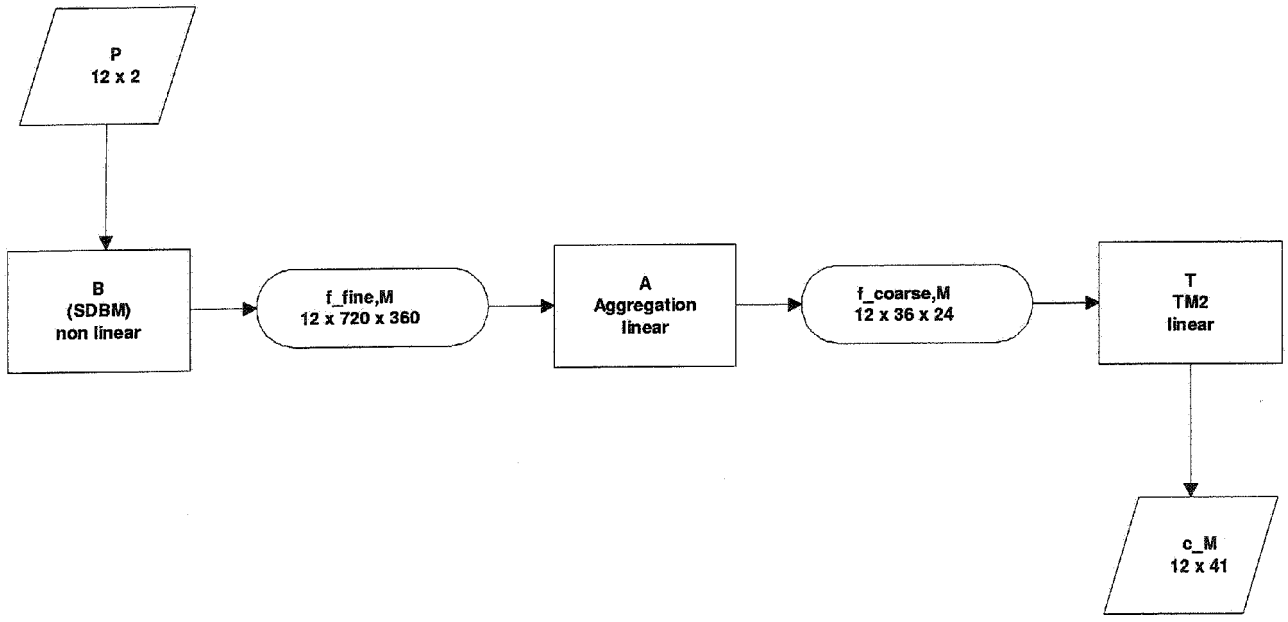

Figure 1. Flow diagram for the forward direction of information in our composite model. Boxes show the various quantities predicted by the chain of models while arrows describe the mappings between these fields.

A. Although this is not important in the abstract description of the problem, it is an important benefit of the method that small-scale forcing of the biosphere can propagate through to the atmospheric concentrations. If we were limited to the rather coarse transport model grid some of the details of this forcing would be lost.

[14] Finally there is the atmospheric transport model which maps fluxes onto atmospheric concentrations. We denote this operator as **T**. The use of the adjoint approach described by *Kaminski et al.* [1999a] means that **T** can take fluxes at the full resolution of the underlying transport model and map them onto a predetermined set of observed concentrations.

[15] Combining the three steps, we have a mapping from biosphere parameters to modeled concentrations $\mathbf{c}_M$ expressed as

$$\mathbf{c}_M = M(\mathbf{p}) = \mathbf{T} \times \mathbf{A} \times B(\mathbf{p}). \quad (1)$$

Strictly, the multiplication in the above expression represents composition of functions. **T** and **A** are linear, however, so we can also consider this as matrix multiplication. We stress again that nowhere in the construction of $\mathbf{c}_M$ do we need to make assumptions about the structure of fluxes apart from those implicit in the biosphere model itself.

[16] We define an optimal vector **p** so that it minimizes the overall mismatch with observed concentrations. To this end we construct a cost function,

$$J_c(\mathbf{p}) = {}^1\!/_2 (M(\mathbf{p}) - \mathbf{c})^T \mathbf{C}_\mathbf{c}^{-1} (M(\mathbf{p}) - \mathbf{c}), \quad (2)$$

where $\mathbf{C}_\mathbf{c}$ expresses our uncertainty for the observations **c** in the form of a covariance matrix. Several augmented forms of J_c are possible representing information from other points along the chain of models. For example, we can add a term embodying a mismatch of **p** from some prior estimate $\mathbf{p}_0$. This is the Bayesian approach. It is normally used in flux inversions such as *Rayner et al.* [1999], partly to stabilize the estimates and partly to embody prior knowledge of fluxes. In our case this knowledge may be embodied in the model instead. Also, if there are observed fluxes, **f**, we can add a term such as

$$J_f(\mathbf{p}) = {}^1\!/_2 (N(\mathbf{p}) - \mathbf{f})^T \mathbf{C}_\mathbf{f}^{-1} (N(\mathbf{p}) - \mathbf{f}), \quad (3)$$

where by analogy with equation (1) we have denoted by N the function that computes modeled fluxes $\mathbf{f_M}$ from **p**. We can replace fluxes by any other observable calculated by the biosphere model.

[17] We are now left with the computational problem of optimizing **p** in the nonlinear composite model M. Note that whatever optimization algorithm we use will involve several, perhaps many, runs of M. This is not feasible if we need to run **T** many times, because **T** is the most expensive part of our model. Since **T** is linear, we can precalculate a set of response functions, the approach normally used in previous synthesis inversions. In our application, this has a serious drawback. We can only calculate the response functions for a subspace of fluxes. Our choice of subspace represents a choice of a set of flux patterns, usually reflecting structure within a particular region. In our case, as we change **p** through the iterative optimization process, these shapes will change. *Kaminski et al.* [2001] showed that incorrect choices of flux shapes could seriously distort an inversion. Fortunately, *Kaminski et al.* [1999a] demonstra-

ted the efficient calculation of the complete response function for a transport model provided we only need modeled concentrations at selected sites and times. Thus we can include the transport model as a simple matrix multiplication without losing the required generality of flux fields.

[18] The calculation of **T** is based on automatic differentiation (AD) of the atmospheric transport model in reverse mode [*Griewank*, 2000]. It is efficient, because the number of input parameters to the model (fluxes at every month and surface grid cell) considerably exceeds the number of output variables (concentrations at every month at about 50 sites). The same observation holds for the interpolation matrix **A**. Hence, again, we have applied AD in reverse mode to generate the adjoint code of the interpolation routine. This adjoint code efficiently computes **A**. The automatic differentiation has been carried out by the Tangent linear and Adjoint Model Compiler (TAMC, R. Giering, 2000, available at http://puddle.mit.edu/~ralf/tamc)).

[19] Powerful minimization algorithms for functions like J, rely on the availability of the gradient of J with respect to the parameters. Hence, again, we apply TAMC in reverse mode to generate a subroutine to evaluate $\nabla_{\mathbf{p}} J(\mathbf{p})$ for any **p**. Unlike the adjoints of **T** and **A** which evaluate derivatives of vector valued functions, the adjoint of J evaluates the derivative of a scalar valued function. This derivative is a fairly compact expression, mapping maybe a few dozen parameters onto their impact on the cost function, even though some of the intermediate fields and hence mappings may be large.

[20] The cost function minimization allows us to calculate an optimal parameter set but provides no information on the uncertainty in those parameters. Some information can be obtained from the value of the second derivative or Hessian at the minimum. Geometrically, this is the curvature of the cost function. A subroutine for evaluation of the Hessian is obtained by reapplying TAMC to the adjoint. It is slightly more efficient to use the forward mode for this second pass, because the function to be differentiated has as many input as output variables (parameters and components of the gradient, respectively).

[21] The way the cost function defined by equations (2) and (3) is set up reflects the assumption of Gaussian probability distributions for the observed concentrations, the fluxes, and the a priori information about the parameters (the Gaussian assumption). If our model was linear, one could show [see, e.g., *Tarantola*, 1987, equations (4.4)–(4.6)] that the posterior probability distribution is Gaussian as well and that the uncertainties in the optimal parameters are quantified by a covariance matrix which is the inverse of the Hessian at the minimum. Since the model is nonlinear, uncertainties derived this way are merely an approximation (the locality approximation). In this work we make yet another approximation, the linearity approximation. We apply TAMC in forward mode to compute the linearizations or Jacobian matrices of the mappings that relate parameters to atmospheric concentrations (M) and fluxes (N) at observational sites. These Jacobians are denoted by $D_{\mathbf{p}}M$ and $D_{\mathbf{p}}N$, respectively. Since in each case there are fewer parameters than observations, the forward mode is computationally preferable. In this linear approximation, the posterior covariance matrix $\mathbf{C}_p$ is given by

$$\mathbf{C}_p^{-1} = (D_{\mathbf{p}}M)\mathbf{C}_c^{-1}(D_{\mathbf{p}}M)^T + (D_{\mathbf{p}}N)\mathbf{C}_f^{-1}(D_{\mathbf{p}}N)^T + \mathbf{C}_{0,p}^{-1}, \quad (4)$$

where $\mathbf{C}_{0,p}$ expresses the a priori uncertainty in parameters. The inverse can be computed, for example, by a singular value decomposition (SVD). We have described the formula and the SVD [*Rayner et al.*, 1999; *Kaminski et al.*, 1999b], but all the background is given by *Tarantola* [1987]. We shall check the locality approximation and the linearity approximation by comparing the cost function generated by varying the parameters around their optimal values with the cost function implied by our calculated parameter uncertainties.

[22] The locality approximation has an important consequence for the calculated uncertainty. As an example, consider a cost function which is quadratic in the region of the optimal values but contains a large potential barrier at zero, effectively disallowing negative values. This might occur if we wish to prevent an optimization routine taking logarithms of negative numbers. Our local analysis of uncertainties at the cost function minimum will never, even in principle, see this constraint. Even with this limitation, the calculation of uncertainties still represents a substantial advance on previous methods.

[23] In the final step of the process, the calculation of fluxes and their uncertainties, we use the optimal values from the first step and the covariance matrix from the second. The flux calculation requires only a forward run of the biosphere model, although to reduce storage requirements we can use the aggregation step to output fluxes on the transport model grid. Note that even here, the covariance matrix representing the uncertainty in flux estimates is very large, $10{,}368 \times 10{,}368$. Fortunately we can store a compact expression for the square root of this matrix and generate relevant fields off-line.

[24] It is worth reiterating the centrality of the automatic differentiation tool TAMC in this whole process. In fact, it is used 5 times. First, we use it to calculate the aggregation operator **A**. Next we use the matrix representation of the transport model TM2 calculated by *Kaminski et al.* [1999a]. The optimization step uses the derivative of the cost function with respect to input parameters, which is provided by the adjoint of the composite model, M. The calculation of approximate parameter uncertainties uses the Jacobian of observations with respect to biosphere parameters, generated as a tangent linear model to the forward model. Finally, the calculation of flux uncertainties uses the Jacobian of fluxes with respect to parameters, again a tangent linear model but this time leaving out the transport model step.

3. Models and Data

3.1. Biosphere Model

[25] We use the Simple Diagnostic Biosphere Model (SDBM) described by *Knorr and Heimann* [1995]. In brief, the model calculates a pure seasonal cycle of net bio-

sphere–atmosphere fluxes as the difference of two fluxes in any month at each 0.5° × 0.5° land grid cell,

$$F = H - NPP, \quad (5)$$

where F is the net flux to the atmosphere, H is the heterotrophic respiration, and NPP is the net primary productivity.

[26] The calculation is performed on the basis of measured Normalized Differential Vegetation Index (NDVI), incoming solar radiation, and surface temperature. There is an additional time-dependent water-stress term α, which may limit the efficiency either of NPP, or heterotrophic respiration, or both. This factor will be included in various of the calculations in this work in either of the two fluxes H and NPP; in the case described below, it is included in both.

[27] NPP is calculated for each month as

$$NPP = \alpha\epsilon APAR, \quad (6)$$

where APAR is absorbed photosynthetically active radiation and ϵ is a light-use efficiency parameter. APAR is computed from NDVI data by *Gallow* [1992] and incoming solar radiation inferred from cloudiness data by *Leemans and Cramer* [1991] using the method of *Linacre* [1968].

[28] Heterotrophic respiration H is calculated as an exponential function of temperature as

$$H = \alpha\epsilon H_0 Q_{10}^{T/10}, \quad (7)$$

where ϵH_0 is the heterotrophic respiration rate at $T = 0$ and $\alpha = 1$ (i.e., no water stress) and Q_{10} is the ratio of respiration at $T + 10$ to that at T; T is given in °C. We have absorbed ϵ into the formulation of H for later convenience.

[29] In order to ensure a balanced biosphere (no net annual flux), we rescale H_0 at each grid cell so that integrated NPP and H are equal over a year. Thus H_0 is not a free parameter.

[30] The water-stress factor, α = AET/PET (actual divided by potential evapotranspiration), is computed with the model of *Prentice et al.* [1993]. PET is assumed equal to equilibrium evapotranspiration, and AET is the minimum of PET and a supply rate assumed proportional to soil moisture. The model neglects the effect of soil freezing and snow accumulation, so that at low ambient temperatures where PET is mostly small, α tends toward 1. Freezing-induced drought effects are therefore not considered in SDBM; low temperatures rather affect H through its temperature dependence given by the value of Q_{10}.

[31] We can now write the total flux as

$$F(t) = \alpha\epsilon\left(H_0 Q_{10}^{T(t)/10} - APAR(t)\right). \quad (8)$$

Subject to the constraint that

$$H_0 \int Q_{10}^{T(t)/10} dt = \int APAR(t) dt, \quad (9)$$

where integrals are taken over the annual cycle. Integrals are calculated as sums of monthly values weighted by the length of the month.

3.2. Transport Model

[32] We use the adjoint form of the transport model TM2. The base model is described by *Heimann* [1995]. The model is an off-line tracer transport model with a 7.8° latitude × 10° longitude grid and nine vertical levels. It is driven by analyzed winds from the European Centre for Medium Range Weather Forecasting (ECMWF), in this case from the year 1987. The model features vertical transport by convection and turbulent eddy transport following the schemes of *Louis* [1979] and *Tiedtke* [1989], respectively.

[33] TM2 was a participant in the Transport Model Comparison (TransCom) project reported by *Rayner and Law* [1995] and *Law et al.* [1996]. Of most importance here was its simulation of the seasonal cycle, since the amplitude and phase of the seasonal cycle are the critical parameters in our study. In general, the simulated seasonal amplitudes lie within the range of other model simulations. One different emphasis of this model is the relatively large amplitudes over tropical regions compared to those over higher latitude regions. We should bear this in mind when considering the distribution of NPP between low and high latitudes in our optimizations. We must stress, of course, that the range of model simulations does not necessarily provide guidance for the correct atmospheric transport behavior.

[34] The adjoint form of the model was constructed by *Kaminski et al.* [1999a] and used in a previous flux inversion by *Kaminski et al.* [1999b]. The adjoint model calculates the derivative of the monthly mean concentration at a specified set of observing sites with respect to emissions in all surface grid points and all months. Since simulated concentrations are linear in emissions, this derivative need only be calculated once. Hence, once we restrict ourselves to a given observing network, the transport model can be replaced by a single matrix multiplication. As we have already mentioned, this form of the transport model allows the full structure of fluxes up to the resolution of the transport model to be mapped onto concentrations. This is an important advantage in a study like ours, since changes in parameters may cause small-scale changes in the structure of fluxes.

3.3. Data

[35] We use the compilations of the seasonal cycle from *GLOBALVIEW-CO_2* [2000]. We use a network of 41 stations. The network we use is shown in Figure 2 and listed in Table 1.

[36] One obvious property of the network is its oceanic focus. This is clearly undesirable for our current study, and one of our aims will be to investigate the knowledge available from such a network for constraining biospheric processes. We have removed the oceanic bias somewhat by eliminating the sampling locations from ship cruises in the Pacific Ocean and South China Sea.

[37] As well as assigning data values, we need to assign an uncertainty for weighting the data in equation (2). We calculate the data uncertainty from the two uncertainty estimates provided by *GLOBALVIEW-CO_2* [2000]. One uncertainty comes from the residuals of the flask data from the smoothed curve used to define the monthly mean. It is a measure of short-term variability and the concomitant sampling error. The other contribution is the interannual variability in the monthly means themselves.

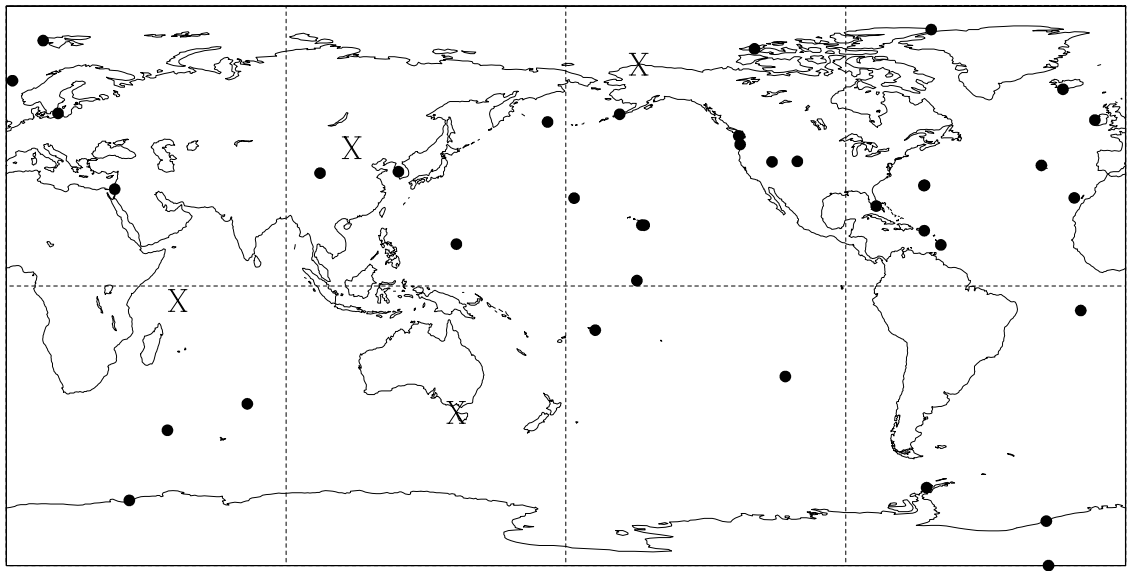

Figure 2. CO_2 observing network used in the study.

[38] While a detailed discussion of the assignment of data uncertainty in synthesis inversions is beyond us here, we note that these uncertainty estimates are really a proxy for a range of uncertainties which must be included in our calculation. These include (1) imprecision in the measurements themselves, (2) the inability to simulate concentrations measured at a point and time with monthly mean model concentrations on a $7.8^\circ \times 10^\circ$ grid, (3) inadequacies in the biosphere or transport model including their driving data and source heterogeneity not captured by the model, and (4) uncertainties in the other contributions to the seasonal cycle which are not included in our statistical model. All these uncertainties are hard to quantify. In particular, uncertainties from source heterogeneity depend critically on the choice of structures which can be resolved by the model, as demonstrated by *Kaminski et al.* [2001]. In general, the data uncertainties from *GLOBALVIEW-CO_2* [2000] have the right structure, with larger errors in the vicinity of large and heterogeneous sources.

[39] In our calculation we quadratically sum the two components of the Globalview uncertainty, since we need to take both into account. Finally, to deal with potential model inadequacies, we require a minimum value of 0.70 ppmv. This minimum value is important, since 328 of the 452 values used in our standard case would otherwise have lower uncertainties. Table 1 lists the root-mean-square uncertainty for each station, averaged over the year.

3.4. Background Fluxes

[40] Terrestrial biospheric activity, particularly the seasonal cycle, is focused on the large land masses of the Northern Hemisphere and tropics. Even here, and particularly in the southern extratropics, the other major carbon fluxes may make a significant contribution to the seasonal cycle of CO_2 concentration. Even seasonality in transport acting on a time-invariant source field may produce substantial seasonality in concentration. We include three such contributions in our study. These extra fluxes should be considered part of the driving data for the problem; that is, we do not optimize them in any way. Note that the seasonal cycle is the main datum which forces our results, so contributions to seasonality are more important than overall magnitude. We must factor uncertainties in the contribution of these fluxes to seasonality of concentration into uncertainties in the data.

[41] We use the annually invariant flux from fossil fuel combustion and cement production compiled by *Andres et al.* [1996]. The seasonality in concentration arising from this flux is largest at low latitudes, peaking around 1 ppmv at Seychelles in our study. Seasonal variations in the flux are likely to produce even smaller seasonality in concentration than this and will hence be unimportant for this study.

[42] We use the estimate of ocean CO_2 flux compiled by *Takahashi et al.* [1999] derived from a compilation of air–sea δpCO_2 values and using the air–sea gas exchange formulation of *Wanninkhof* [1992]. This field contains moderate seasonality and in the Southern Hemisphere is likely to be a major contributor to seasonality in the concentration records. However, in the Northern Hemisphere and tropics, its maximum values around 1 ppmv are only a small contribution to the observed seasonal cycle. Thus, while there may be errors in the seasonality of the flux estimates, these probably do not contribute much to the overall seasonality in concentration.

[43] Finally, we use the estimate of flux due to land-use change compiled by *Houghton et al.* [1990]. Strictly, this considers only the source due to deforestation rather than land abandonment. It is focused on low latitudes. Most importantly, for our study we treat it as annually invariant, whereas the burning events which comprise this flux largely occur in the tropical dry season, in reality. Thus, there may be a significant error in seasonality in this flux, and we

Table 1. List of Station Codes and Names Along With Their RMS Uncertainties and RMS Errors for the Control Optimization

Code	Descriptive Name	RMS Uncertainty, ppmv	RMS Error, ppmv
ALT	Alert, N.W.T., Canada	0.73	1.25
AMS	Amsterdam Island	0.70	0.58
ASC	Ascension Island	0.70	0.54
AVI	St. Croix, Virgin Islands	0.71	1.10
AZR	Terceira Island, Azores	0.96	0.62
BAL	Baltic Sea	2.79	0.73
BME	St. David's Head, Bermuda	0.83	1.19
BMW	Southhampton, Bermuda	0.96	1.22
BRW	Barrow, Alaska	0.81	1.59
CBA	Cold Bay, Alaska	0.83	1.26
CGO	Cape Grim, Tasmania	0.70	0.48
CHR	Christmas Island, Kiribati	0.70	0.50
CMO	Cape Meares, Oregon	1.22	0.72
CRZ	Crozet, Indian Ocean	0.70	0.44
EIC	Easter Island	0.70	0.68
GMI	Guam, Mariana Islands	0.74	0.61
HBA	Halley Bay, Antarctica	0.70	0.27
ICE	Storhofdi, Heimaey, Vestmannaeyjar, Iceland	0.77	1.02
IZO	Tenerife, Canary Islands	0.70	0.65
KEY	Key Biscayne, Florida	0.81	0.95
KUM	Cape Kumukahi, Hawaii	0.70	0.84
MBC	Mould Bay, N.W.T., Canada	0.77	1.42
MHD	Mace Head, Ireland	0.84	1.22
MID	Sand Island, Midway	0.73	0.71
MLO	Mauna Loa, Hawaii	0.70	0.39
NWR	Niwot Ridge, Colorado	0.81	1.10
OPW	Olympic Peninsula, Washington	1.24	0.78
PSA	Palmer Station, Antarctica	0.70	0.18
RPB	Ragged Point, Barbados	0.70	1.24
SEY	Mahe Island, Seychelles	0.70	0.53
SHM	Shemya Island, Alaska	0.89	1.46
SMO	Tutuila, American Samoa	0.70	0.32
SPO	South Pole, Antarctica	0.70	0.20
STM	Atlantic Ocean (Polarfront)	0.75	1.50
SYO	Syowa Station, Antarctica	0.70	0.32
TAP	Tae-ahn Peninsula, Korea	2.25	0.31
UTA	Wendover, Utah	1.19	0.80
UUM	Ulaan Uul, Mongolia	1.12	1.05
WIS	Sede Boker, Israel	1.03	1.90
WLG	Mt. Waliguan, China	0.86	1.37
ZEP	Zeppelin Station, Svalbard	0.86	0.98

should consider this when interpreting results for low-latitude biomes.

3.5. Implementation Details

[44] In this work we aim to estimate the two parameters ϵ (light-use efficiency) and Q_{10} in SDBM for each of 12 biomes. The biomes are taken from *DeFries and Townshend* [1994], and their distribution is shown in Figure 3. Abbreviations used throughout the paper for each biome are listed in Table 2. This generates 24 unknowns of interest. As well, we need to solve for a mean value at each of the stations in our chosen observational network. Although we use the pure seasonal cycles from *GLOBALVIEW-CO_2* [2000], and SDBM generates a pure seasonal cycle, the composite model will compute nonzero mean values for two reasons. First, we must consider the contributions to the seasonal cycle made by fossil-fuel combustion and ocean fluxes; these are input as known fluxes. Second, the covariance of transport and seasonal biospheric fluxes will of itself produce a nonzero mean value, as demonstrated by *Keeling et al.* [1989], *Denning et al.* [1995], and *Law et al.* [1996]. To avoid this mismatch producing erroneous corrections to biosphere parameters, we use a free-floating offset to match the mean value. Thus we have one extra unknown per station in the observing network. These offsets are only important in the optimization step, and we neglect them later.

[45] Throughout the following calculations, we use a Bayesian estimation Procedure; that is, we include prior constraints on the biosphere parameters but not on the offsets. Prior uncertainties for the ϵ are set at 50% of their initial value while those for Q_{10} are set at 30% of their prior value, as shown in Figures 4 and 5.

4. Results

[46] In this section we will discuss two major aspects of the results of optimizations using the framework described above. First, we will show some of the estimated parameters and fluxes produced by our control case and some variations of it. Then we will discuss the uncertainties on these parameters, with a view to recovering the information on biospheric processes available from atmospheric concentration observations.

[47] For our control case, we choose an inversion with the water-stress parameter α turned on for both the NPP and respiration terms. Figures 4 and 5 show the prior and predicted values of ϵ and Q_{10} for each biome in our standard inversion. Several things are immediately apparent from these figures. First, the ϵ values are generally shifted further from their prior estimates than the Q_{10} parameters. This would normally be expected because of the generally larger reduction in uncertainty in ϵ, which indicates that the inversion is adding more information about ϵ than about Q_{10}. The proximate cause for this difference is the greater sensitivity of the seasonal cycle of concentrations to changes in ϵ than Q_{10}. This is a direct result of the model formulation as can be seen from the governing equations of SDBM (equation (8)) and the nature of the forcing functions for the model. As formulated, the amplitude of the seasonal cycle of flux in SDBM is governed by the value of ϵ. The phase results from the interaction of seasonal variations in temperature and water stress with the value of Q_{10}. With the seasonality of temperature and water stress fixed, there is relatively little sensitivity of fluxes to changes in Q_{10} and hence only a weak constraint on this parameter.

[48] The structure of the changes to ϵ also shows some interesting features. In general, ϵ is increased for high-latitude biomes. In Particular, the optimization suggests that the high-latitude deciduous forests and tundra require high light-use efficiency to match seasonality in concentration. The coniferous forest (also mostly found at high latitudes) has optimized ϵ closer to the prior value. The tundra and deciduous forest values are particularly striking since their optimized confidence interval is shifted outside or nearly outside their original confidence interval. Meanwhile, the C4 grassland biome has its light-use efficiency parameter reduced almost to zero.

[49] When considering the above results, it is useful to take into account the relative biological importance of the

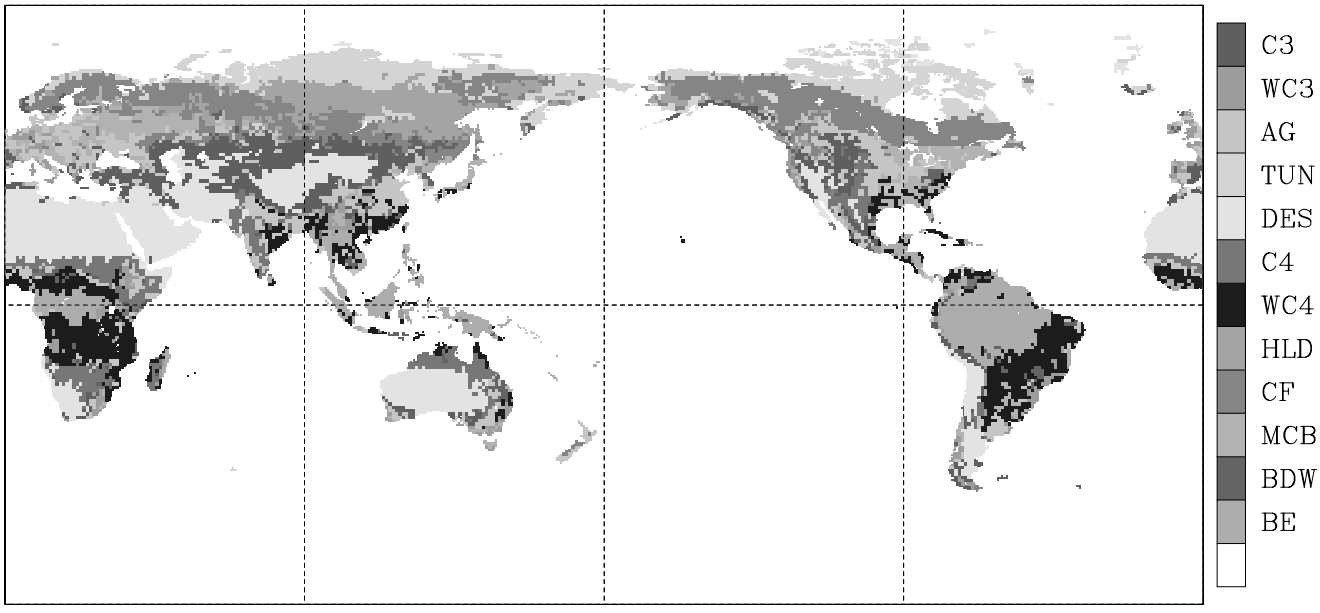

Figure 3. Distribution of biomes used in the study, taken from *DeFries and Townshend* [1994]. Biome labels are described in Table 2. See color version of this figure at back of this issue.

various biomes. A measure of this importance is the total APAR associated with each biome, or, alternatively, its total NPP. Figure 6 shows the prior and predicted NPP for each biome. The prior uncertainties reflect the 50% prior uncertainty on ϵ. The global total is hardly changed from the prior estimate (53.8 to 53.5 Gt C). The uncertainty is reduced, from 11 to 7.2 Gt C which is approximately 13% of the total. This reduction in uncertainty suggests only moderate scope for concentration measurements used alone to constrain such large-scale processes.

[50] This result resembles that of *Knorr and Heimann* [2001], who used satellite-derived vegetation index data to constrain a global process-based vegetation model. They estimated error margins for the most important model parameters and performed a series of sensitivity studies. The result was that without the satellite constraint, the model was inconsistent with the observed seasonal cycle of atmospheric CO_2. Consistency was improved after inversion against the satellite data. The uncertainty in global NPP for the free model, which would correspond to SDBM with prior parameters and uncertainties, was 24.1 Gt C from a total of 75.8 Gt C (31%), while the model consistent with both satellite and CO_2 data still had 18.5 Gt C uncertainty out of 73.6 Gt C (25%). Apart from the fact that uncertainties can be expected to be larger for a process-based model that has many more parameters, their result again stresses the importance of using multiple constraints for optimizing global vegetation models. It should also be noted that the station network used by *Knorr and Heimann* [2001] was smaller than the one in the present study, and that their analysis used tropical stations only in a qualitative way.

[51] Figure 6 shows that some of the largest changes in ϵ occur for biomes with relatively small NPP. In particular, the large decrease for the C4 grassland biome and large increase for tundra do not have dramatic effects, since their total NPP is relatively small. Uncertainties for ϵ for these biomes also remain close to their prior value. One reason for this is evident from equation (6). As the signal in the atmosphere used to constrain the model is created by the seasonal cycle of net flux, F (equation (5)), and because of the way H_0 is calculated, this signal scales linearly with ϵ. How sensitive the seasonal cycle is to changes in ϵ, however, depends on the seasonal cycle in α (tropical biomes), in T (northern biomes), and APAR (both). As noted by Knorr and *Heimann* [1995], the seasonal cycle in the tropics is very small when α is included in both NPP and H. This means that the seasonal cycle of concentrations that we observe is not sensitive to ϵ from the C4 grassland biome. Such a lack of sensitivity means that the parameter is only weakly constrained. In fact, *Knorr and Heimann* [2001] found that tropical trees and C4 grasses make a sizeable contribution to the seasonal cycle only south of the equator (15 and 25%, respectively), where this seasonal cycle is small.

[52] Another diagnostic output of the model is the spatial distribution of NPP. This can be compared with the NPP

Table 2. Descriptive Abbreviations Used for Biomes

Abbreviation	Full Name
BE	broadleaf evergreen
BDW	broadleaf deciduous and woodland
MCB	mixed coniferous, broadleaf deciduous, and woodland
CF	coniferous forest and woodland
HLD	high lat deciduous and woodland
WC4	wooded C_4 grassland
C4	C_4 grassland
DES	shrubs and bare ground (desert)
TUN	tundra
AG	cultivation (agriculture)
WC3	C_3 wooded grassland
C3	C_3 grassland

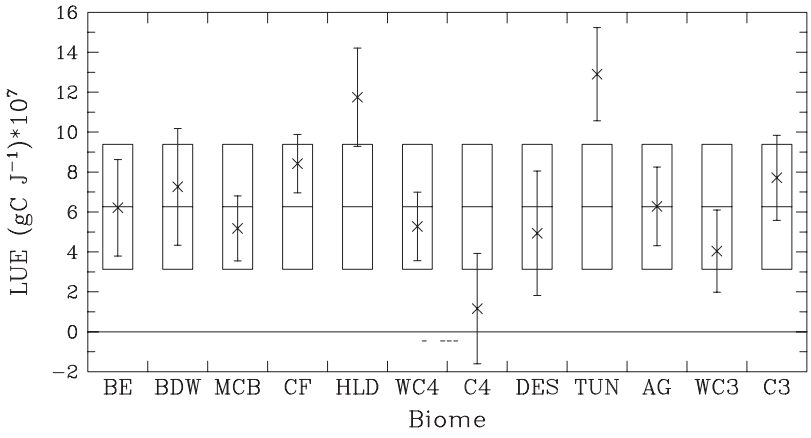

Figure 4. Light-use efficiency ϵ for 12 biomes. The horizontal line shows the prior estimate, the box shows 1 standard deviation of prior uncertainty, the cross shows the optimized value, and the error bar

fields produced by other calculations. In the Potsdam Intercomparison [*Cramer et al.*, 1999], many terrestrial modeling groups produced such estimates. Figure 7 shows the zonal mean NPP per unit land area for four optimized cases for SDBM along with the median and extreme deciles from *Kicklighter et al.* [1999]. The four optimized cases show the impact of including water stress for either or both of NPP and respiration. We see that our standard case (water stress on for both) lies close to the median value in the tropics but above the upper decile in high northern latitudes. This is consistent with the observation of *Nemry et al.* [1999] that most of the models in the Potsdam Intercomparison underestimated seasonality of concentrations at high latitudes. This is also true for initial parameter settings of SDBM, so the optimization increases ϵ in high latitudes to improve the match. NPP is increased as a consequence.

[53] Low-latitude NPP shows great sensitivity to the treatment of water stress. While our standard case lies close to the median Potsdam result, all the other cases lie below the lowest decile. There is less sensitivity elsewhere, suggesting either that NPP is so low that the range is tightly constrained (subtropics), or that water stress is not a serious factor in controlling NPP (high latitudes). These results are consistent with Knorr and *Heimann* [1995], who showed that the impact of water stress on seasonal cycles of concentration could only be noticed from tropical regions.

[54] As we have already noted, the most striking facet of the Q_{10} results in Figure 5 is the large predicted uncertainties on this value. This weak constraint occurs despite the use of biomes representing large regions; it would be worse at finer spatial resolution. Hence any comment we make on the predicted estimates must be rather cautious. One general feature that does emerge is the tendency for high values for high-latitude biomes and lower values for tropical biomes. All biomes suggest a positive sensitivity of heterotrophic respiration to air temperature ($Q_{10} > 1$) consistent with the measurements compiled by *Raich and Potter* [1995], which also refer to air temperature. When soil respiration is related to soil temperature, however, Q_{10} values are mostly higher, closer to the commonly assumed value of 2, as reported by *Raich and Schlesinger* [1992]. However, the median of the values found experimentally by *Holland et al.* [2000] for

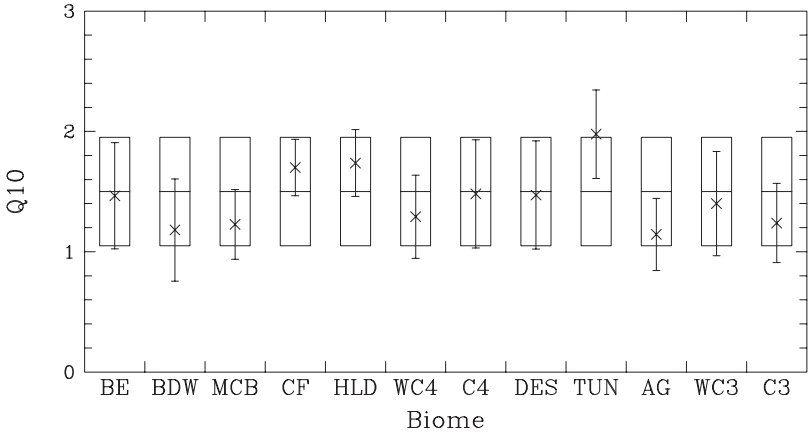

Figure 5. Q_{10} for twelve biomes. The horizontal line shows the prior estimate, the box shows 1 standard deviation of prior uncertainty, the cross shows the optimized value, and the error bar shows 1 standard deviation of predicted uncertainty. Biome labels are described in Table 2.

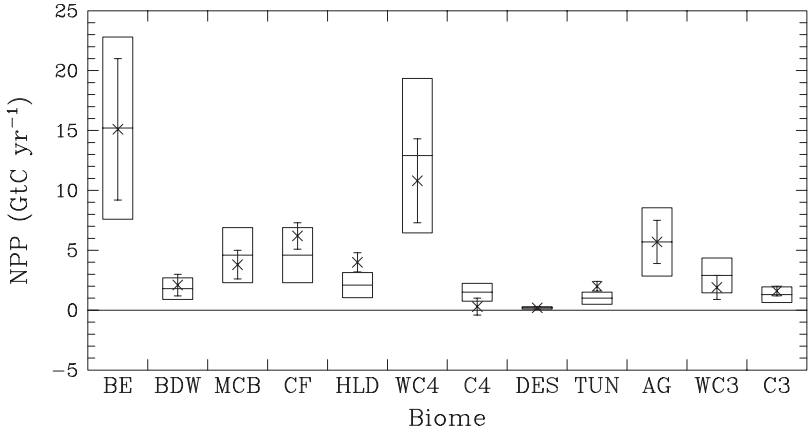

Figure 6. NPP for 12 biomes. The horizontal line shows the prior estimate, the box shows 1 standard deviation of prior uncertainty, the cross shows the optimized value, and the error bar shows 1 standard deviation of predicted uncertainty. Biome labels are described in Table 2.

tropical soils (1.74) still lies within the confidence interval for the tropical biomes.

[55] To study the impact of extra measurements in this calculation we repeated the standard case with the addition of some pseudoflux measurements. These fake measurements were created by archiving the fluxes for one point in the Broadleaf Evergreen biome, then recalculating the propagated uncertainties. Since the pseudoflux data is that from the optimized model itself, the estimated values do not change. We assign the monthly mean pseudoflux data an uncertainty of 10 gm^{-2}month^{-1}, corresponding to an error of approximately 5% of the maximum monthly flux. This uncertainty should be regarded as an example, particularly as we have not included the representativeness of such a flux for the entire biome. Overall uncertainties for both ϵ and Q_{10} in this biome are much reduced. Figure 8 shows the

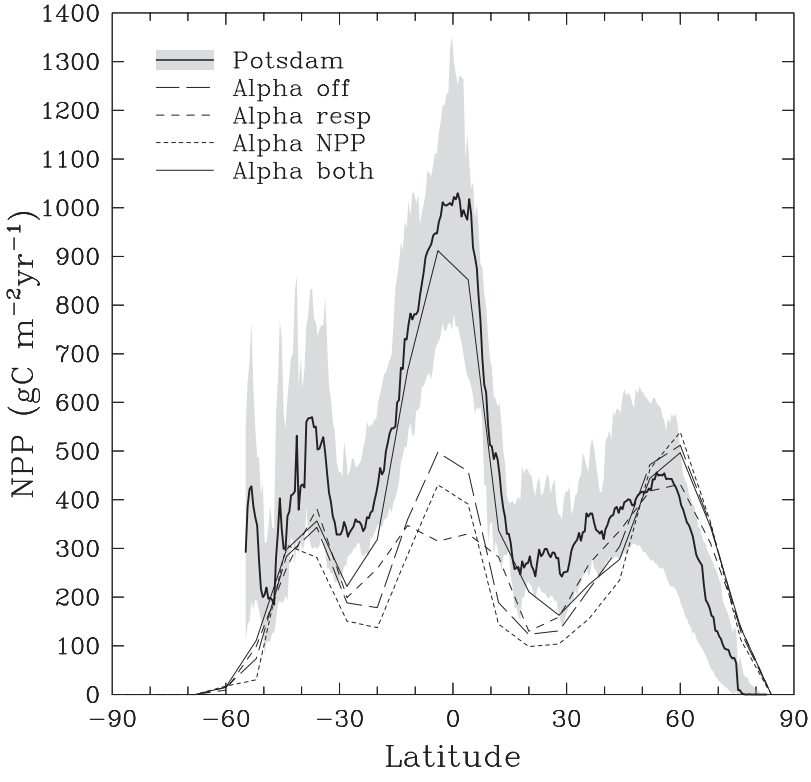

Figure 7. Zonal mean NPP per unit land area for four cases. The solid line shows our standard case while the three dashed lines show cases where the effect of water stress is turned off for either or both of NPP and respiration. Line styles are as shown in the key. The shading indicates the interdecile range of model estimates from the Potsdam Intercomparison while the bold line shows the median.

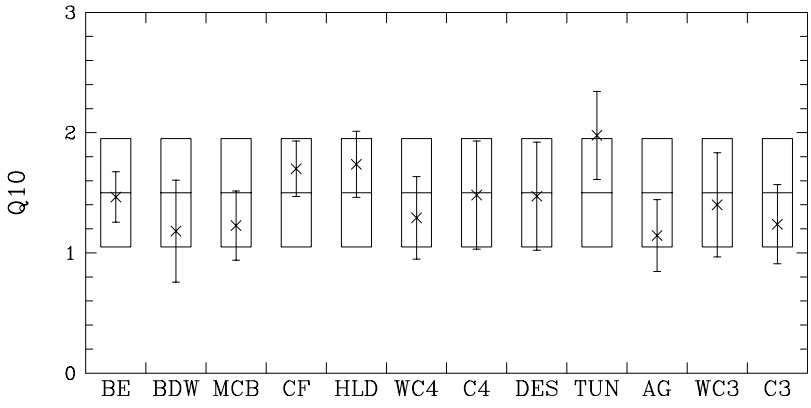

Figure 8. Predicted Q_{10} with the addition of a pseudoflux measurement in the broadleaf evergreen biome. The pseudoflux data is that predicted from optimized values for that point and the flux measurement uncertainty is 10 g m^{-2} yr^{-1}. The horizontal line shows the prior estimate, the box shows 1 standard deviation of prior uncertainty, and the cross shows the optimized value. The vertical bar shows the 1 standard deviation confidence interval of the predicted value. Biome labels are described in Table 2.

results for Q_{10}. The uncertainty of Q_{10} for the broadleaf evergreen biome that was not well constrained by concentration observations is substantially reduced. This complimentary role suggests combined use of both types of measurements.

[56] SDBM is a very simple model of seasonal carbon exchange. It is worthwhile asking, then, how well it can fit the concentration observations when its parameters are optimized. As examples, Figure 9 shows the predicted and observed seasonal cycle for four stations: Point Barrow, Alaska; Ulaan Uul, Mongolia; Mahe Island, Seychelles; and Cape Grim Tasmania. These are marked on Figure 2. The dashed lines either side of the observed line show the uncertainty used on each monthly datapoint. The same information is also summarized in Table 1, where the final column shows the root-mean-square error (rmse) between predicted and observed concentration from our control case. Barrow is one of the worst simulated stations (rmse = 1.59 ppmv). It's large seasonal cycle, of course, provides some context for this error. The general phase and amplitude of the seasonal cycle are well simulated. The clearest error is an overestimate of the source during spring. Notwithstanding this, the optimized and even unoptimized model produces more accurate seasonality at high latitudes than many models with more sophisticated biogeochemistry but less diagnostic information [see, e.g., *Nemry et al.*, 1999].

[57] At Ulaan Uul (rmse =1.05 ppmv), the general form of the seasonal cycle is well simulated, the only error being a slight overestimate of the amplitude. The much smaller seasonal cycle at Seychelles is also fairly well simulated (rmse = 0.53 ppmv). Errors are larger as a proportion of the seasonal cycle, but the data uncertainties are similarly proportionally larger. Seasonality at Seychelles is driven by combinations of seasonality from nearby land and complex modulations of large-scale transport such as monsoon circulations and the movement of the intertropical convergence zone (ITCZ). Simulations with only the background (fossil and ocean) fluxes suggest these may contribute as much to the seasonal cycle at Seychelles as the biosphere, which suggests both that our conservative choice of data uncertainties is wise and that this is not a good site to try to constrain tropical biomes.

[58] Finally, the even smaller seasonality evident at Cape Grim is fairly well simulated by the model (rmse = 0.48 ppmv). The amplitude is roughly correct, but the model leads the observations by perhaps 2 months. Here there might be a case for much tighter uncertainty bounds on the observations, but the uncertain contribution of the background fluxes (the ocean in particular here) would support our more conservative choice. *Law* [1996] also showed considerable sensitivity of the phase of the seasonal cycle at Cape Grim to methods used to select clean or baseline air, already pointed out in the original analysis with SDBM by *Knorr and Heimann* [1995].

[59] We can calculate a global measure of the quality of the optimal simulation as the mean-square mismatch or χ^2 value,

$$\chi^2 = \frac{1}{N}\sum_{i=1}^{N}\left(\frac{c_{M,i} - c_{c,i}}{\sigma_i}\right)^2 = J_c 2N, \qquad (10)$$

where $c_{M,i}$ is modeled concentration, c_{ci} is observed concentration, and σ_i is the prior uncertainty on the observed concentration. N is the total number of concentration observations. In general, if our statistical assumptions are valid, χ^2 will be around 1. It should at least not be greater than 1, or we should suspect that our prior uncertainties are too tight.

[60] The χ^2 value gives us a convenient summary measure of the quality of a given optimization. Table 3 shows this mismatch along with the global NPP and NPP for each biome from the four optimization cases from Figure 7. The table reinforces the behavior seen in the figure, notably that NPP is much lower for the tropical biomes (BE and WC4) in our alternative cases than the control. This lowers the global NPP, also. It is interesting that including the impact of water stress on respiration when it already effects photosynthesis (the last two columns) has the most dramatic impact on optimized NPP of any single parameter change. This occurs despite the assumption in the model that, at every point, annual respiration is adjusted to balance NPP.

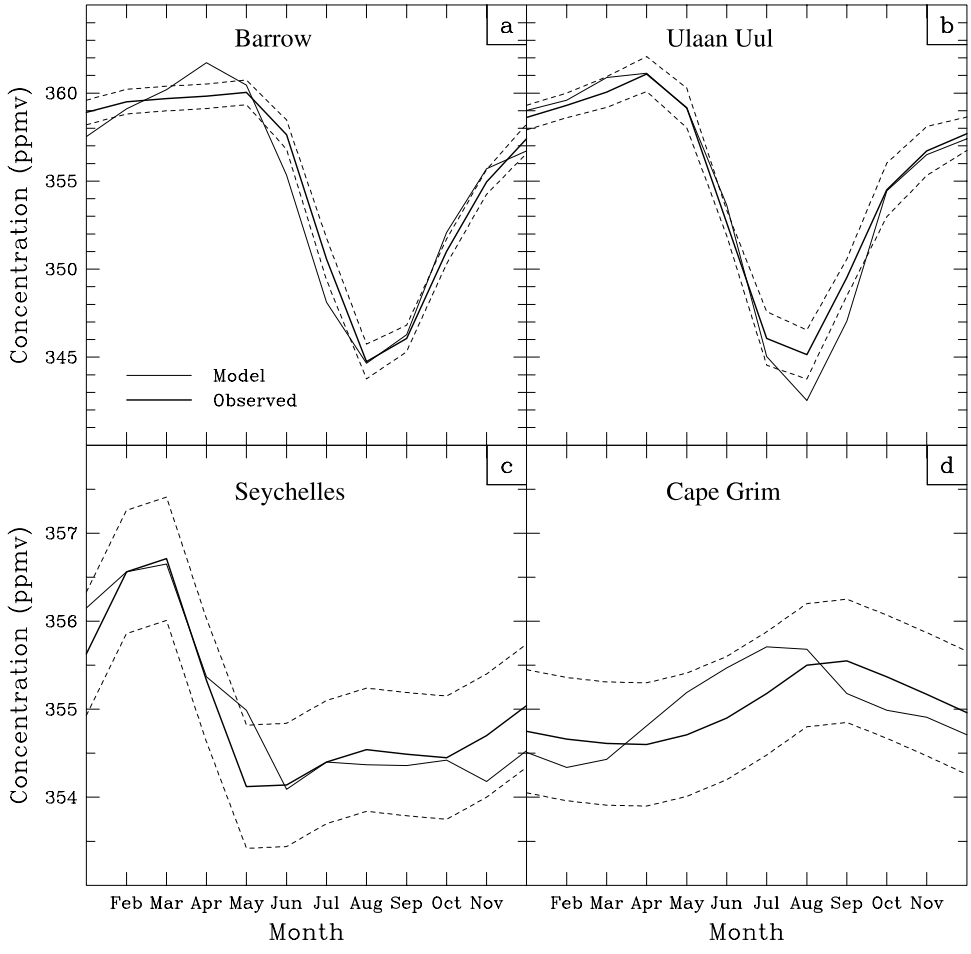

Figure 9. Simulated and observed seasonal cycle of concentration (ppmv) for four observing sites: (a) Point Barrow Alaska, (b) Ulaan Uul, Mongolia, (c) Mahe Island, Seychelles, and (d) Cape Grim, Tasmania. The dashed line indicates ±1 standard deviation about the observations.

A similar result was previously noted by *Lloyd and Farquhar* [1994] and *Knorr and Heimann* [1995] for Q_{10}. A larger Q_{10} value, they noted, increases the proportion of respiration in summer and hence requires a larger NPP to produce the large drawdown in summer concentrations. In our case, water stress reduces respiration in the dry season and so requires a smaller value of ϵ to avoid a large drawdown. The mismatch is not very sensitive to the presence of α, although we see that, as suggested by Knorr and *Heimann* [1995], the match is worst when water stress is considered to impact NPP but not respiration.

[61] As a final example, Figures 10 and 11 show the terrestrial biospheric fluxes for July and their uncertainties as calculated from the optimal parameter values and their uncertainties. The overall structure of the fluxes is as one might expect for July, with large uptake over the high-latitude continents decreasing at lower latitudes and, generally, sources in the Southern Hemisphere. The uncertainty in fluxes generally scales with the flux, suggesting that uncertainties in ϵ are the main contributor to flux uncertainty, at least for this month. There is also a role for correlations between parameters in reducing uncertainties on net flux. This role is only possible because of the propagation of the complete covariance structure through the calculation.

[62] We can compare the power of this technique with the traditional inversion of atmospheric transport by comparing the flux uncertainties we calculate to those from the transport inversion at comparable resolution reported by *Kaminski et al.* [1998, Figure 23]. That study, using a 25-station network, achieved small reductions in uncertainty at the grid-point level, usually much less than 5%. In contrast, our July case has flux uncertainties roughly proportional to uncertainties in ϵ. Thus we can predict the uncertainty reduction for fluxes from the uncertainty reduction for ϵ. For most biomes, this reduction is much greater than 5%. This higher reduction in uncertainty is a consequence of the additional constraint introduced through the biosphere model. The result is unsurprising given the relatively small parameter set we are optimizing.

5. Discussion

[63] Given the extreme simplicity of SDBM, it is questionable how much weight to put on the particular results of our optimization. The ability to simulate the observed data,

Table 3. Predicted NPP for Various Model Configurations[a]

	NPP, Gt C					
	Prior		Optimized			
Biome Abbrev	α-off	α-NPP	α-off	α-resp	α-NPP	α-both
BE	16.0	15.2	8.0	3.3	6.8	14.6
BDW	2.1	1.8	2.1	2.4	1.9	2.1
MCB	5.0	4.6	6.2	3.7	5.6	3.7
CF	5.0	4.6	6.2	3.7	7.0	5.7
HLD	2.2	2.1	4.0	4.1	4.3	4.1
WC4	14.4	12.9	4.8	7.5	3.5	10.9
C4	2.0	1.5	−0.3	0.9	−0.5	0.3
DES	0.4	0.2	0.3	0.3	0.2	0.2
TUN	1.0	1.0	1.9	2.1	1.6	2.0
AG	6.7	5.7	4.8	8.6	3.9	6.1
WC3	3.2	2.9	2.2	0.3	3.0	2.2
C3	1.9	1.3	0.9	2.7	−1.0	1.6
Global	60.0	53.8	41.1	39.5	36.4	53.5
Mismatch	n/a	n/a	0.87	0.78	0.98	0.87

[a]Headings refer to whether water stress α is included for each flux component. Columns two and three list the unoptimized NPP for two model configurations, the first with water stress (α) turned off and the second including its effect on NPP (control case). Columns four through seven list NPP for four optimized model configurations, including or excluding the effect of water stress on photosynthesis or respiration. Biome abbreviations are listed in Table 2.

while a necessary condition for the use of the model, should not be taken as a validation of the optimized values. We have not performed a detailed cross-validation study here, which would involve simulating concentrations we do not use in the optimization and comparing them with observations. Such a study would be required before we placed great weight on the results. As we have already stated, the technique is an attempt to build process understanding explicitly into atmospheric inversions; if the process understanding is oversimplified, the conclusions will be correspondingly erroneous.

[64] All this having been said, some of the general structure of the results is interesting. The overall value of Q_{10} is lower than studies relating soil respiration to soil temperature [e.g., *Raich and Schlesinger*, 1992], but similar to those that use air temperature [e.g., *Raich and Potter*, 1995]. This difference has also been noted by other studies using atmospheric forcing to drive terrestrial models [e.g., *Maisongrande et al.*, 1997; *Randerson et al.*, 2002]. It most likely results from the difference between soil and air temperatures. The dominant process in heterotrophic respiration, respiration from within soils, presumably reacts to soil temperature. Soil tends to damp the large variations in air temperature, either diurnally or seasonally. Snow has a particularly strong effect on the seasonal variations. Thus the apparent sensitivity of respiration to air temperature is lower than it would be for soil temperature.

[65] The latitudinal structure of Q_{10} is also interesting, although the uncertainties make strong conclusions unwise. In general, the above argument would suggest a closer match between soil-temperature and air-temperature derived values of Q_{10} at low latitudes than at high latitudes, since air temperature variations are so much higher at high latitudes. We, however, observe higher values at high latitudes than low in agreement with *Maisongrande et al.* [1997]. Our result also agrees with the finding by *Holland et al.* [2000] that many tropical soils show values below 2, less than the typical values for northern latitudes cited by *Raich and Schlesinger* [1992].

[66] We have already noted a similar gradient in optimized values of ϵ with latitude. The implied structure in NPP is clearly at variance with the consensus understanding of terrestrial biological models as shown in Figure 7. There are several potential explanations for this. One possibility is the impact of processes that may affect the seasonal cycle but are not included in the model. These include seasonality in disturbance fluxes. Most of these (e.g., fires) would be expected to counteract the strong summer drawdown of atmospheric CO_2 and hence require even larger values of ϵ to match the observed seasonal cycle of concentrations. More likely is the model's assumption about the relationship

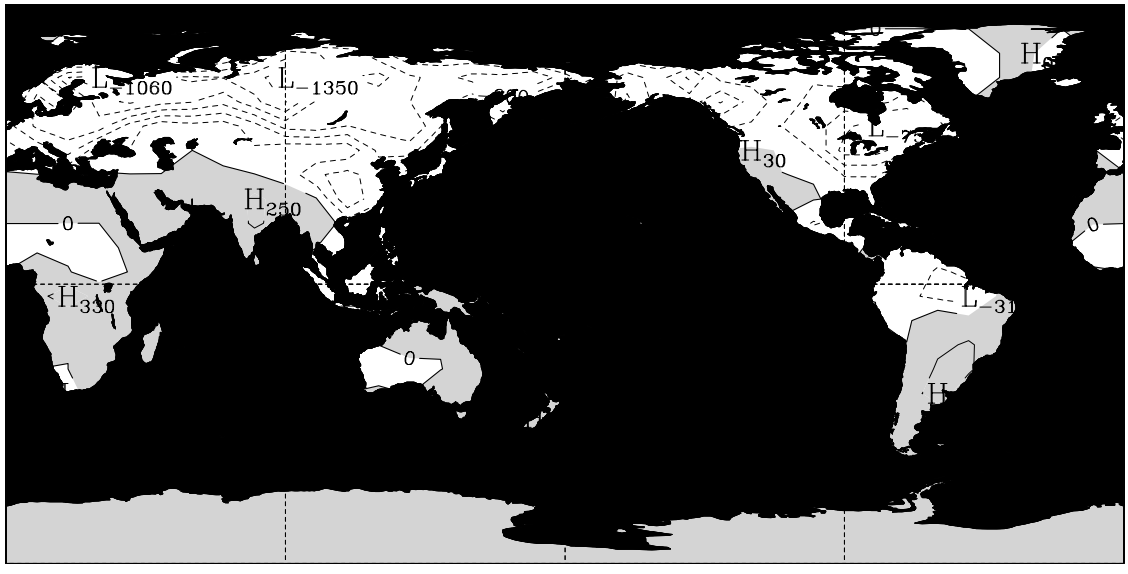

Figure 10. Predicted monthly mean net flux (g C m^{-2} yr^{-1}) from land for July in the control case. The contour interval is 200 and positive values are shaded.

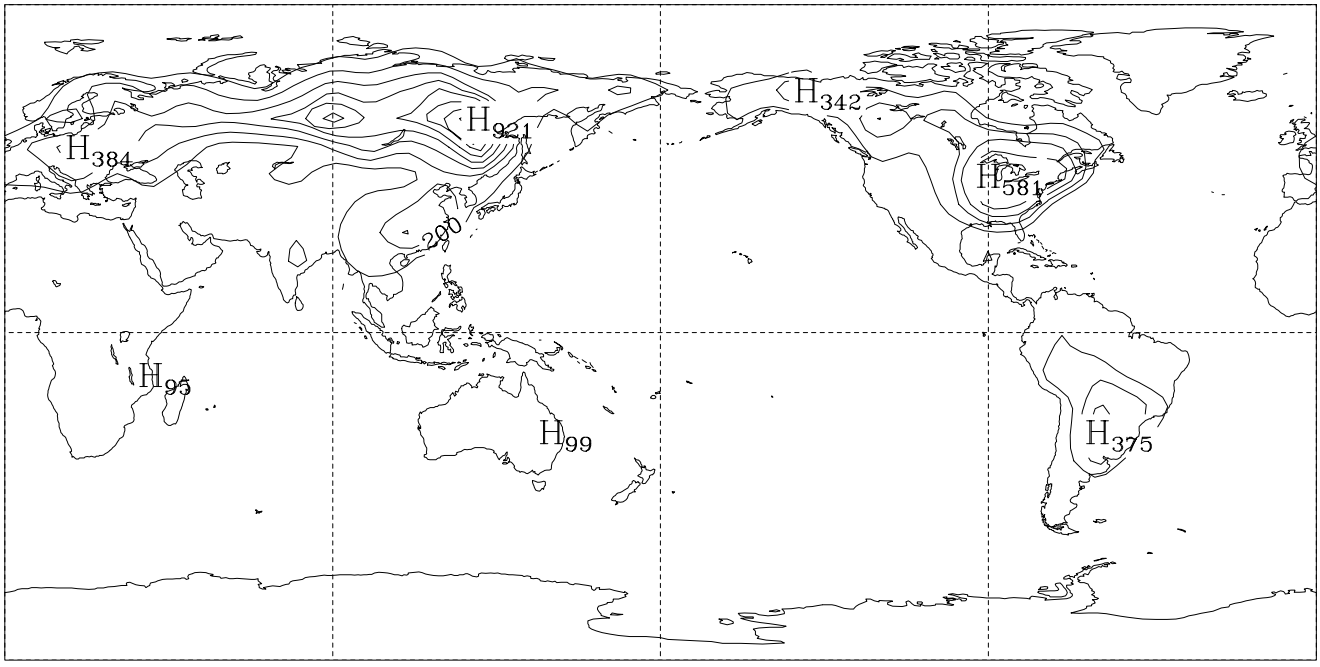

Figure 11. Predicted standard deviation for net flux (g C m^{-2} yr^{-1}) from land for July in the control case. The contour interval is 100.

between seasonal and annual mean production. Here these are governed by the one parameter ϵ. Increasing ϵ to match the seasonal cycle of concentration necessarily increases annual NPP. Possibilities like reducing minimum NPP to achieve the same increase in seasonality are not available to the model. Similarly, annual mean NPP depends on the relationship between annual mean APAR and its seasonality. For example, the seasonality in NPP is unaffected by adding a constant value to every monthly APAR value, but the annual mean NPP will change. The effect on the monthly net flux is complicated by the constraint of a balanced biosphere.

[67] There is a more fundamental issue facing the approach outlined in this paper which transcends any particular results. It concerns the propagation of constraints from one series of measurements across large and spatially separate regions. This is a common concern in terrestrial biological modeling, often (though confusingly) referred to as the scaling problem. In our calculations the issue is most starkly demonstrated by the influence of flux measurements taken at a specific point throughout an entire biome. Recall that a fictitious measurement on a single $0.5^\circ \times 0.5^\circ$ grid cell produced a substantial reduction in uncertainty in productivity for an entire large biome. This is inherent in the use of single parameters to describe entire biomes. The idea is challenged by a recent study by *Wang et al.* [2001], who optimized parameters in their biophysical model against campaign-mode flux observations taken at several apparently similar sites. They calculated large variations in photosynthetic capacity challenging the very idea of applying parameters on large scales. We should note that the model used in that study did not consider differences in nutrient status between the various sites, so that in some sense their model was not complete.

[68] This objection is certainly serious, but has implications far beyond inversion studies like this. However it is stated, the aim of local measurements is to garner process understanding and apply it more widely. If this generalization is in principle impossible, then a major motivation for such measurements is invalid. In its broadest sense the inability to translate understanding from one place to another represents model failure. Whether this failure is inevitable and insoluble remains an open question. The framework outlined here provides a method for testing such questions, since local or process-based estimates can be generalized and rigorously compared with integral constraints such as atmospheric concentration observations. Any operational use of such a procedure would involve quarantining some observations from the optimization procedure to check (or cross-validate) the inferences we might make.

[69] Finally, there are some aspects of the uncertainty calculations shown throughout this paper which require further comment. These concern the propagation of uncertainty through our linearized model to yield multivariate normal distributions for our inferred parameters from multivariate normal distributions of our observables. This is an inherent limitation of our analysis. As noted in section 2, we make the linearity approximation of calculating the derivative of the cost function via the derivative of concentrations with respect to parameters rather than by direct calculation of the Hessian. We can test this approximation by comparing the cost function as a function of one parameter to the ideal cost function assuming the normal distribution computed by linear error propagation. Figure 12 shows an example of such a comparison, for Q_{10} for the broadleaf evergreen biome. We note good agreement in the curvature around the minimum. This agreement suggests that our

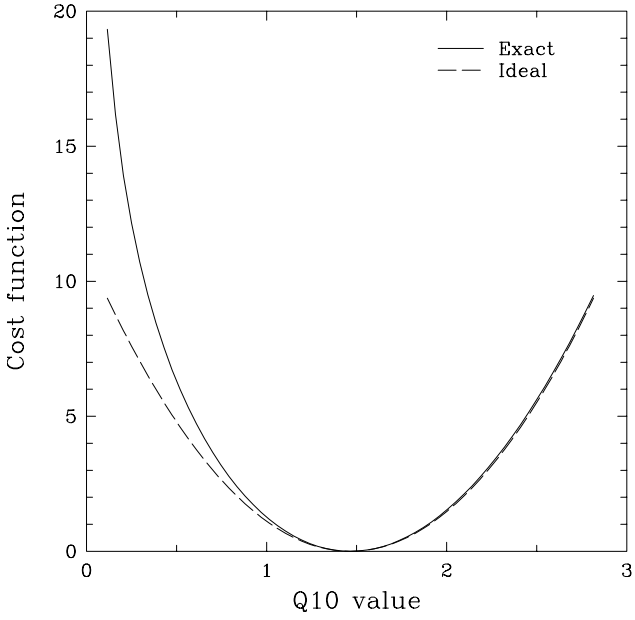

Figure 12. Exact and ideal marginal cost function for Q_{10} for the Broadleaf Evergreen biome. The ideal cost function is calculated from the mean and standard deviation for this parameter from the optimization. The exact cost function is calculated by varying the parameter and running the model.

uncertainty estimate is locally correct, i.e., that our linearity approximation is a good one. Figure 12 also provides a test of our locality approximation. Were the real cost function purely quadratic (corresponding to a Gaussian posterior distribution), this agreement would not only hold near the minimum, but across all values. However, we see a more rapid increase in cost for low Q_{10} values in the real than the ideal cost function, reflecting that our ideal probability distribution overestimates the probability of low Q_{10} values. This disagreement might partly explain the relatively low Q_{10} values seen in this study, since the mean Q_{10} value from the real probability distribution would be larger than from the ideal.

[70] The simplicity of the problem studied in this paper is mainly driven by the simplicity of the terrestrial biosphere model we employ. The simplicity manifests itself in two important aspects. First, the model calculates only the seasonal cycle of fluxes. With the dominant focus of research in the carbon cycle now shifting to understanding the climate sensitivity of the underlying source processes, there is an obvious opening to repeat this work with a model capable of simulating interannual variability of fluxes. In particular, it would be interesting to see how much confidence in predictions of terrestrial biosphere responses to climate change can be improved by parameter calibrations against the historical record. Another consequence of the simplicity of the biosphere model is that prior uncertainties only enter two parameters, although in a more realistic, process-based model, many more parameters would have to be specified. This has been explored in detail by *Knorr and Heimann* [2001], and the result is an approximate doubling of uncertainties in global annual NPP compared to this study.

[71] The other important limitation of this model is its limited set of observables. This meant we could not do a real comparison of local and integral measures. The work of *Knorr and Heimann* [2001] suggests that other forms of data may constrain terrestrial biosphere models more strongly than the atmospheric concentrations used here. Models which simulated, rather than were driven by, absorbed photosynthetically active radiation as well as fluxes and stock changes might yield a much more stringent test of whether the framework outlined here is useful in real situations. The use of such satellite-derived data has been investigated by *Knorr and Schulz* [2001] and *Knorr and Heimann* [2001], and a preliminary assimilation study combining these with concentration observations is presented by *Rayner et al.* [2001].

6. Conclusions

[72] We have outlined and demonstrated an assimilation framework for combining atmospheric concentration measurements with local measurements in constraining a terrestrial biosphere model. Using the Simple Diagnostic Biosphere Model and the techniques of automatic differentiation, we have been able to constrain the net primary productivity globally and in most major biomes using the seasonal cycle of atmospheric concentration. The results generally show higher light-use efficiencies in high latitudes than low latitudes, a consequence of the unoptimized model's failure to match the seasonal cycle in concentration at high latitudes. Predicted NPP for the base case is close to the median of the Potsdam Intercomparison at low latitudes and higher at high northern latitudes. Low-latitude NPP is sensitive to the treatment of water stress in SDBM with three variations that we tested, showing substantially lower NPP than our base case. The sensitivity of heterotrophic respiration to temperature is poorly constrained by concentration measurements but better constrained by local flux pseudodata. Finally, the calculated uncertainties on fluxes for July suggest that the method may be useful in constraining tropical terrestrial fluxes from the sparse observing network. This constraint relies on using the process model to extrapolate information gained in one region throughout large biomes. This is a more soundly based approach than the previous flux-based inversions but is subject to the veracity of the terrestrial model.

[73] **Acknowledgments.** This study was carried out with the support of the Bundesministerium für Bildung und Forschung (BMBF) contract 01LA9898/9. The authors wish to thank Rachel Law for helpful comments on the manuscript.

References

Andres, R. J., G. Marland, I. Fung, and E. Matthews, A $1° \times 1°$ distribution of carbon dioxide emissions from fossil fuel consumption and cement manufacture, 1950–1990, *Global Biogeochem. Cycles*, *10*, 419–429, 1996.

Balkanski, Y., P. Monfray, M. Battle, and M. Heimann, Ocean primary production derived from satellite data: An evaluation with atmospheric oxygen measurements, *Global Biogeochem. Cycles*, *13*, 257–271, 1999.

Cramer, W., D. W. Kicklighter, A. Bondeau, B. I. Moore, G. Churkina, A. Ruimy, A. L. Schloss, and J. Kaduk, Comparing global models of terrestrial net primary productivity (NPP): Overview and key results, *Global Change Biol.*, *5*, 1–15, 1999.

DeFries, R. S., and J. R. G. Townshend, NDVI-derived land cover classifications at a global scale, *Int. J. Remote Sens.*, *15*, 3567–3586, 1994.

Denning, A. S., I. Y. Fung, and D. A. Randall, Gradient of atmospheric CO_2 due to seasonal exchange with land biota, *Nature*, *376*, 240–243, 1995.

Enting, I. G., C. M. Trudinger, and R. J. Francey, A synthesis inversion of the concentration and $\delta^{13}C$ of atmospheric CO_2, *Tellus, Ser. B*, *47*, 35–52, 1995.

Fung, I. Y., C. J. Tucker, and K. C. Prentice, Application of Advanced Very High Resolution Radiometer vegetation index to study atmosphere–biosphere exchange of CO_2, *J. Geophys. Res.*, *92*, 2999–3015, 1987.

Gallow, K. P., Experimental global vegetation index from AVHRR utilizing pre-launch calibration, cloud and sun-angle screening, Digital Data, Natl. Geophys. Data Cent., Natl. Oceanic and Atmos. Admin., Boulder, Colo., 1992.

GLOBALVIEW-CO_2, Cooperative Atmospheric Data Integration Project—Carbon Dioxide [CD-ROM], Natl. Oceanic and Atmos. Admin. Clim. Monit. and Diag. Lab., Boulder, Colorado, 2000. (Available on Internet via anonymous FTP to ftp.cmdl.noaa.gov, Path: ccg/CO_2/GLOBALVIEW)

Gloor, M., S. M. Fan, S. Pacala, and J. Sarmiento, Optimal sampling of the atmosphere for purpose of inverse modeling: A model study, *Global Biogeochem. Cycles*, *14*, 407–428, 2000.

Griewank, A., *Evaluating Derivatives: Principles and Techniques of Automatic Differentiation*, Soc. For Indust. and Appl. Math., Philadelphia, Pa., 2000.

Heimann, M., The global atmospheric tracer model TM2, *Tech. Rep. 10*, Dtsch. Klimarechenzentrum, Hamburg, Germany, 1995.

Holland, E. A., J. C. Neff, A. R. Townsend, and B. McKeown, Uncertainties in the temperature sensitivity of decomposition in tropical and subtropical ecosystems: Implications for models, *Global Biogeochem. Cycles*, *14*, 1137–1151, 2000.

Houghton, J. T., , G. J. Jenkins, and J. J. Ephraums (Eds.), *Climate Change: The IPCC Assessment*, Cambridge Univ. Press, New York, 1990.

Kaminski, T., M. Heimann, and R. Giering, A matrix representation for an atmospheric transport model computed by its adjoint, in *Air Pollution Modelling and its Application XII*, edited by S.-E. Gryning and N. Chaumerliac, pp. 247–255, Plenum, New York, 1998.

Kaminski, T., M. Heimann, and R. Giering, A coarse grid three-dimensional global inverse model of the atmospheric transport, 1, Adjoint model and Jacobian matrix, *J. Geophys. Res.*, *104*, 18,535–18,553, 1999a.

Kaminski, T., M. Heimann, and R. Giering, A coarse grid three-dimensional global inverse model of the atmospheric transport, 2, Inversion of the transport of CO_2 in the 1980s, *J. Geophys. Res.*, *104*, 18,555–18,581, 1999b.

Kaminski, T., P. J. Rayner, M. Heimann, and I. G. Enting, On aggregation errors in atmospheric transport inversions, *J. Geophys. Res.*, *106*, 4703–4715, 2001.

Keeling, C. D., S. C. Piper, and M. Heimann, A three-dimensional model of atmospheric CO_2 transport based on observed winds, 4, Mean annual gradients and interannual variations, in *Aspects of Climate Variability in the Pacific and the Western Americas*, *Geophys. Monogr.*, vol. 55, edited by D. H. Peterson, pp. 305–363, AGU, Washington, D. C., 1989.

Keeling, C. D., T. P. Whorf, M. Wahlen, and J. van der Plicht, Interannual extremes in the rate of rise of atmospheric carbon dioxide since 1980, *Nature*, *375*, 666–670, 1995.

Kicklighter, D. W., A. Bondeau, A. L. Schloss, J. Kaduk, and A. D. McGuire, Comparing global models of terrestrial net primary productivity (NPP): Global pattern and differentiation by major biomes, *Global Change Biol.*, *5*, 16–24, 1999.

Knorr, W., and M. Heimann, Impact of drought stress and other factors on seasonal land biosphere CO_2 exchange studied through an atmospheric tracer transport model, *Tellus, Ser. B*, *47*, 471–489, 1995.

Knorr, W., and M. Heimann, Uncertainties in global terrestrial biosphere modeling, II, Global constraints for a process-based vegetation model, *Global Biogeochem. Cycles*, *15*, 227–246, 2001.

Knorr, W., and J.-P. Schulz, Using satellite data assimilation to infer global soil moisture and vegetation feedback to climate, in *Remote Sensing and Climate Modeling: Synergies and Limitations*, *Adv. in Global Change Res. Ser.*, edited by M. Beniston and M. Verstraete, pp. 273–306, Kluwer Acad., Norwell, Mass., 2001.

Law, R., The selection of model-generated CO_2 data: a case study with seasonal biospheric sources, *Tellus, Ser. B*, *48*, 474–486, 1996.

Law, R. M., et al., Variations in modeled atmospheric transport of carbon dioxide and the consequences for CO_2 inversions, *Global Biogeochem. Cycles*, *10*, 783–796, 1996.

Leemans, R., and W. Cramer, The IIASA climate database for mean monthly values of temperature, precipitation and cloudiness on a terrestrial grid, *Tech. Rep. 91-18*, Inst. of Appl. Syst. Anal., Laxenburg, Austria, 1991.

Linacre, E. T., Estimating the net-radiation flux, *Agric. Meteorol.*, *5*, 49–63, 1968.

Lloyd, J., and G. D. Farquhar, ^{13}C discrimination during CO_2 assimilation by the terrestrial biosphere, *Oecologia*, *99*, 201–215, 1994.

Louis, J. F., A parameteric model of vertical eddy fluxes in the atmosphere, *Boundary Layer Meteorol.*, *17*, 187–202, 1979.

Maisongrande, P., G. Dedieu, A. Ruimy, L. Kergoat, B. B. Saugier, and P. Ciais, Diagnostic and prognostic modeling of the terrestrial biosphere with remotely sensed measurements, in *The Global Carbon Cycle and the Terrestrial Biosphere*, edited by G. Dedieu and J. L. Probst, *Sci. Geol. Bull.*, *50*, 33–58, (unknown), 1997.

Nemry, B., L. François, J. C. Gérard, A. Bondeau, and M. Heimann, Comparing global models of terrestrial net primary productivity (NPP): Analysis of the seasonal atmospheric CO_2 signal, *Global Change Biol.*, *5*, 65–76, 1999.

Prentice, I. C., M. T. Sykes, and W. Cramer, A simulation model for the transient effects of climate change on forest landscapes, *Ecol. Modell.*, *65*, 51–70, 1993.

Raich, J. W., and C. S. Potter, Global patterns of carbon dioxide emissions from soils, *Global Biogeochem. Cycles*, *9*, 23–36, 1995.

Raich, J. W., and W. H. Schlesinger, The global carbon dioxide flux in soil respiration and its relationship to vegetation and climate, *Tellus, Ser. B*, *44*, 81–99, 1992.

Randerson, J. T., et al., The ^{13}C discrimination of arctic and boreal biome net CO_2 exchange inferred from remote atmospheric measurements and a biosphere–atmosphere model, *Global Biogeochem. Cycles*, *16*, 1028, doi:10.1029/2001GB001435, 2002.

Rayner, P., Atmospheric perspectives on the ocean carbon cycle, in *Global Biogeochemical Cycles in the Climate System*, edited by E. D. Schulze et al., pp. 285–294, Academic, San Diego, Calif., 2001.

Rayner, P. J., and R. M. Law, A comparison of modelled responses to prescribed CO_2 sources, *Tech. Pap. 36*, CSIRO Div. of Atmos. Res., Melbourne, Victoria, Australia, 1995.

Rayner, P. J., and D. M. O'Brien, The utility of remotely sensed CO_2 concentration data in surface source inversions, *Geophys. Res. Lett.*, *28*, 175–178, 2001.

Rayner, P. J., I. G. Enting, R. J. Francey, and R. L. Langenfelds, Reconstructing the recent carbon cycle from atmospheric CO_2, $\delta^{13}C$ and O_2/N_2 observations, *Tellus, Ser. B*, *51*, 213–232, 1999.

Rayner, P., W. Knorr, M. Scholze, R. Giering, T. Kaminski, M. Heimann, and C. L. Quërë, Inferring terrestrial biosphere carbon fluxes from combined inversions of atmospheric transport and process-based terrestrial ecosystem models, paper presented at 6th CO2 Conference, Cent. for Atmos. and Oceanic Stud., Tohoku Univ., Sendai, Japan, 1–5 Oct. 2001.

Takahashi, T., R. H. Wanninkhof, R. A. Feely, R. F. Weiss, D. W. Chipman, N. Bates, J. Olafsson, C. Sabine, and S. C. Sutherland, Net sea–air CO_2 flux over the global oceans: An improved estimate based on the sea–air pCO_2 difference, paper presented at 2nd International CO2 in the Oceans Symposium, Cent. for Global and Environ. Res., Natl. Inst. for Environ. Stud., Tsukuba, Japan, 18–22 January 1999.

Tans, P. P., I. Y. Fung, and T. Takahashi, Observational constraints on the global atmospheric CO_2 budget, *Science*, *247*, 1431–1438, 1990.

Tarantola, A., *Inverse Problem Theory: Methods for Data Fitting and Parameter Estimation*, Elsevier, New York, 1987.

Tiedtke, M., A comprehensive mass flux scheme for cumulus parameterization in large-scale models, *Mon. Weather Rev.*, *117*, 1779–1800, 1989.

Vukićević, T., B. H. Braswell, and D. Schimel, A diagnostic study of temperature controls on global terrestrial carbon exchange, *Tellus, Ser. B*, *53*, 150–170, 2001.

Wang, Y. P., R. Leuning, H. Cleugh, and P. A. Coppin, Parameter estimation in surface exchange models using non-linear inversion: How many parameters can we estimate and which measurements are most useful?, *Global Change Biol.*, *7*, 495–510, 2001.

Wanninkhof, R., Relationship between wind speed and gas exchange over the ocean, *J. Geophys. Res.*, *97*, 7373–7383, 1992.

M. Heimann and W. Knorr, Max-Planck-Institut für Biogeochemie, Postfach 100164, D-07701 Jena, Germany. (mheimann@bgc-jena.mpg.de; wknorr@bgc-jena.mpg.de)

T. Kaminski, FastOpt, Martinistrasse 21, D-20251Hamburg, Germany. (thomas@fastopt.de)

P. Rayner, CSIRO-DAR, PMB 1 Aspendale, Victoria 3195, Australia. (peter.rayner@csiro.au)

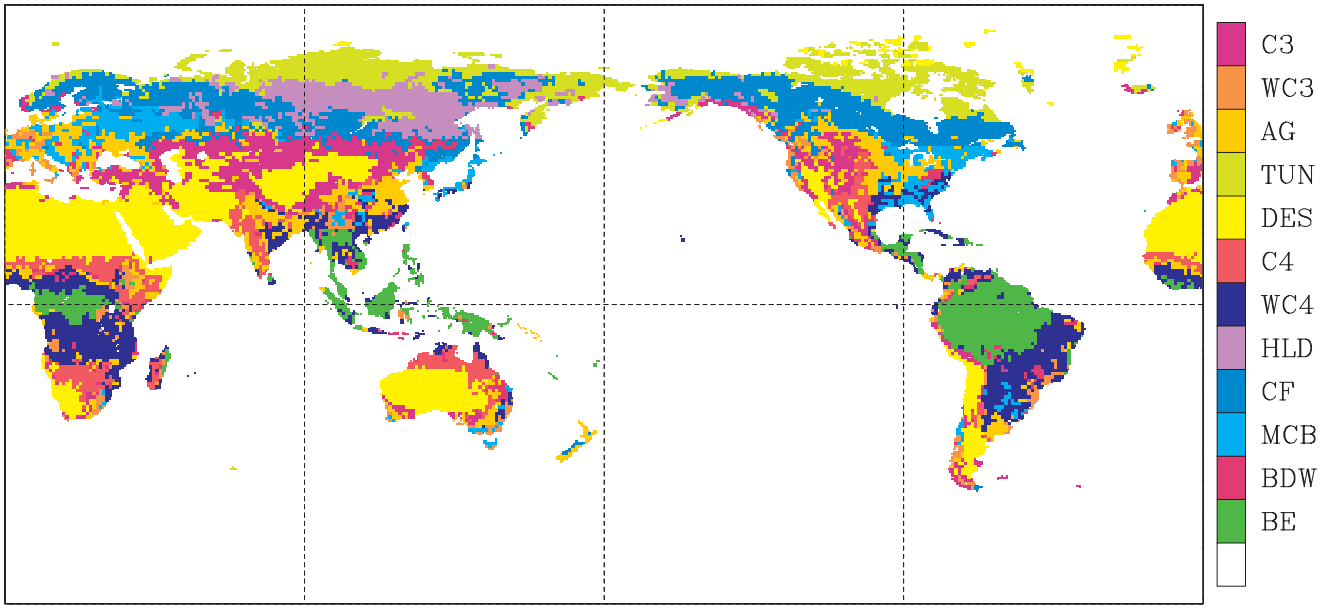

Figure 3. Distribution of biomes used in the study, taken from *DeFries and Townshend* [1994]. Biome labels are described in Table 2.